Available online at www.pelagiaresearchlibrary.com

Pelagia Research Library

Advances in Applied Science Research, 2013, 4(2):286-297

ISSN: 0976-8610
CODEN (USA): AASRFC

Investigation on physico-chemical properties of semiorganic nonlinear optical L-lysine sulphate single crystal

J. Suja Rani[1], M. Meena[2], C. K. Mahadevan[2], M. Antony Arockiaraj[3], S. Rajasekar[4], M. Vimalan[4*] and K. Jaya Kumari[5]

[1]*Department of Physics, Lekshmipuram college of Arts and Science, Neyyoor, India*
[2]*Department of Physics, S.T. Hindu college, Nagercoil, India*
[3]*Department of Physics, Loyola College, Chennai, India*
[4]*Department of Physics, Syed Ammal Engineering College, Ramanathapuram, India*
[5]*Department of Physics, Sree Ayappa College for Women, Chunkankadai, India*

ABSTRACT

Single Crystals of L-lysine sulphate (abbreviated as LLS), a semiorganic nonlinear (NLO) materials have been successfully grown by slow solvent evaporation solution growth technique at room temperature. Solubility curve of LLS has been determined in mixed solvent of acetone and water. The grown crystal is characterized by single crystal X-ray diffraction (XRD) and Fourier transform infrared spectroscopic analysis. The UV–Vis transmittance spectrum shows that the material has low optical absorption in the entire visible region. The relative second harmonic generation is confirmed by Kurtz powder technique. Electrical conductivity measurements are carried out on LLS crystals at various temperatures. Photoconductivity studies of LLS reveals that it exhibits negative photoconductivity.

INTRODUCTION

Recent advances in semiorganic nonlinear optical (NLO) materials have invoked a large revival of interest in this area of research on account of their widespread industrial potential applications in the field of optoelectronics, photonics, telecommunication, optical computing, optical storage and optical information process [1,2]. Nonlinear optical (NLO) process provides the key function of frequency conversion and optical switching devices [3]. In the field of nonlinear optical crystal growth, amino acids play a vital role. Amino acid based organic crystals are interesting materials for NLO applications due to the fact that all the amino acids have molecular chirality, wide transparency ranges in the visible and UV spectral region and zwitterionic nature of the molecule [4]. Complexes of amino acids with inorganic salts are promising materials for optical second harmonic generation (SHG) as they tend to combine the advantages of organic amino acid and inorganic salt. Organic materials are often formed by weak Van der Waals and hydrogen bonds and hence possess a high degree of delocalization. However, these organic crystals have certain limitations such as poor mechanical and thermal stabilities. To overcome these problems, the research of combination of organic and inorganic hybrid compounds lead to find a new class of materials for electronic industries, called semiorganic materials. In semiorganic materials the organic ligand is ionically bonded with inorganic host, because of this, the new semiorganic crystals are having higher mechanical strength and chemical stability. These versatile behaviours of amino acid based semiorganic crystal attract the researchers towards crystal growth of NLO crystals [5]. There are several amino acids crystals that seem to be promising materials as a nonlinear optical generator. Crystalline salts of optically active such as L-arginine, L-histidine, L-lysine, etc., have been intensively studied for NLO applications. Extensive investigations in this direction resulted in the discovery of a series of L-lysine based amino acid compounds. The vibrational spectra and SHG studies of L-lysine with L-tartaric, D, L-malic, acetic, arsenous, and fumaric acids were reported by Marchewka et al [6]. In this series, L-lysine sulphate (LLS) have been recently crystallized and their structural, optical and mechanical properties

have been investigated [7]. The crystal structure of the title compound has already been reported [8]. The present investigation deals with the growth of LLS single crystal by slow solvent evaporation technique. The grown crystal has been subjected to XRD, FT-IR, UV–vis-NIR, SHG, dielectric, photoconductivity and *ac*/*dc* conductivity studies. The results of these investigations are discussed.

MATERIALS AND METHODS

2.1. Synthesis

L-lysine sulphate (LLS) single crystals were grown using solution growth technique at room temperature. To obtain a solution of LLS, appropriate amounts of L-lysine (AR grade) and sulphuric acid (AR grade) were dissolved in mixed solvent of acetone and deionised water (1:1). The chemical reaction between L-lysine and sulphuric acid is as follows.

$$C_6H_{14}N_2O_2 + H_2SO_4 \rightarrow C_6H_{16}N_2O_2^{2+} \cdot SO_4^{2-}$$

The synthesized salt was purified by the repeated crystallization process.

2.2. Solubility

The solubility of LLS in a mixture of acetone and water has been determined for six different temperatures, 30, 35, 40, 45, 50 and 55 ºC, respectively and shown in Fig 1. The solubility data were determined by dissolving the synthesized salt of LLS in 100 ml mixed solvent of acetone-water at a constant temperature with continuous stirring. After attaining saturation, the equilibrium concentration of the solute was analyzed gravimetrically. The same procedure was repeated for different temperatures. The solubility curve of LLS is shown in Fig. 1. The solubility was found to be 6.75 g/100 ml at 30 ºC. Supersaturated solution of LLS was prepared in accordance with the solubility data.

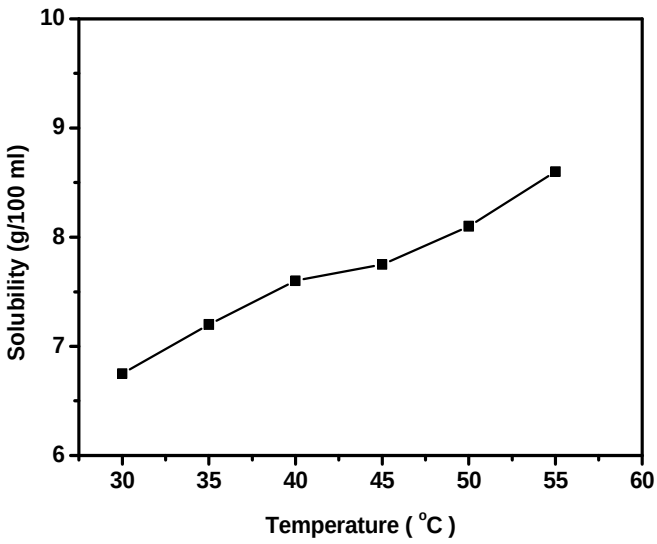

Fig. 1. Solubility curve of LLS

2.3. Growth of LLS Single Crystals

Single crystals of LLS have been grown from saturated solution of the synthesized salt of LLS by the slow evaporation solution growth technique at room temperature. The crystals with perfect shape and free from macro-defects were formed by spontaneous nucleation in the saturated solution. Good optical grade crystals of dimension up to 10 x 8 x 5 mm^3 were conveniently grown in a period of 30 days. Fig. 2 shows the photographs of as grown crystals of LLS.

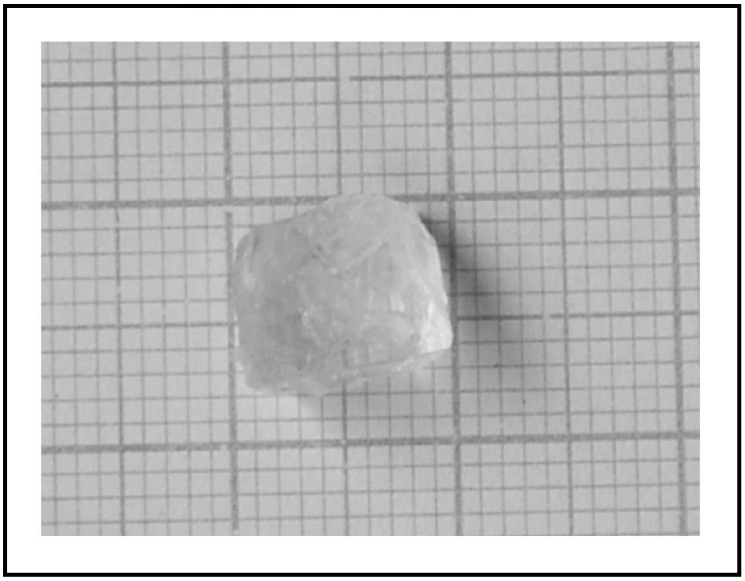

Fig. 2. Photograph of as grown LLS single crystal

3. CHARACTERIZATION

Single crystal X-ray diffraction (XRD) analysis on LLS crystal was carried out using an ENRAF NONIUS CAD4-F diffractometer with MoKα radiation. The coordination of L-lysine with sulphuric acid was confirmed by FT-IR studies using BRUKER IFS 66V FT-IR SPECTROMETER in the range 4000-400 cm^{-1}. The optical absorption spectrum of LLS single crystals has been recorded in the region 200–1100 nm using a Shimadzu UV-1061 UV–vis-NIR spectrometer. The NLO efficiency of LLS crystal was evaluated by Kurtz and Perry powder technique [9] using a Q-switched, mode locked Nd : YAG laser. The *ac* conductivity, dielectric constant and dielectric loss of the LLS sample were studied at room temperature using HIOKI 3532-50 LCR HITESTER in the frequency range 100 Hz to 5 MHz. The measurements of *dc* electrical conductivity were done using the conventional two-probe technique for temperatures ranging from 308 to 368 K. The photocurrent and darkcurrent of the crystal was measured using Keithley 485 picoammeter and the experiment was performed at room temperature.

RESULTS AND DISCUSSION

4.1. X-ray Diffraction Analysis

The crystal data of LLS single crystal were collected by subjecting the grown samples to single crystal XRD and the studies reveals that LLS crystal is orthorhombic and it belongs to $P2_12_12_1$ space group. The calculated lattice parameter values are a = 5.572 Å, b = 11.535 Å, c = 16.595 Å and V = 1066.62 $Å^3$. The XRD data is found to be in good agreement with the reported work [8].

4.2. FT-IR Analysis

Fig. 3 shows the FT-IR transmission spectrum of LLS crystal in the region 4000-400 cm^{-1}. The sample was prepared by mixing it with KBr. Broad absorption band in the 3700-2500 cm^{-1} region is assigned to superimposed O-H and NH_3^+ stretching bands. Absorption in this region is characterized by multiple fine structures on the lower wave number side of the band. The weak band at 3385 cm^{-1} indicates the presence of the asymmetric vibrations of the NH_3^+ group. The symmetric stretching vibrations are found at 3091 cm^{-1} as a medium band in FT-IR. The overtone band around 2417 cm^{-1} is due to combination of the asymmetrical NH_3^+ bending (1620 cm^{-1}) and the torsional oscillation of the NH_3^+ group (595 cm^{-1}). The very strong C-O symmetric stretching vibration of the carboxyl group is observed at 1220 cm^{-1}. The normal modes of vibration in an isolated SO_4 tetrahedron can be identified by the presence of two strong bands in the 1450–1300 and 1200–1100 cm^{-1} regions, due to the asymmetric and symmetric stretching vibrations respectively. The bands are observed at 1432, 1356, 1220 and 1180 cm^{-1}. This corroborates the symmetry lowering of SO_4 in the solid state. The intense medium band at 1030 cm^{-1} is due to C-N stretching mode. The frequency assignment for LLS with various functional groups is presented in Table 1. These vibrations clearly demonstrate the existence of L-lysine in its salt form with sulphuric acid.

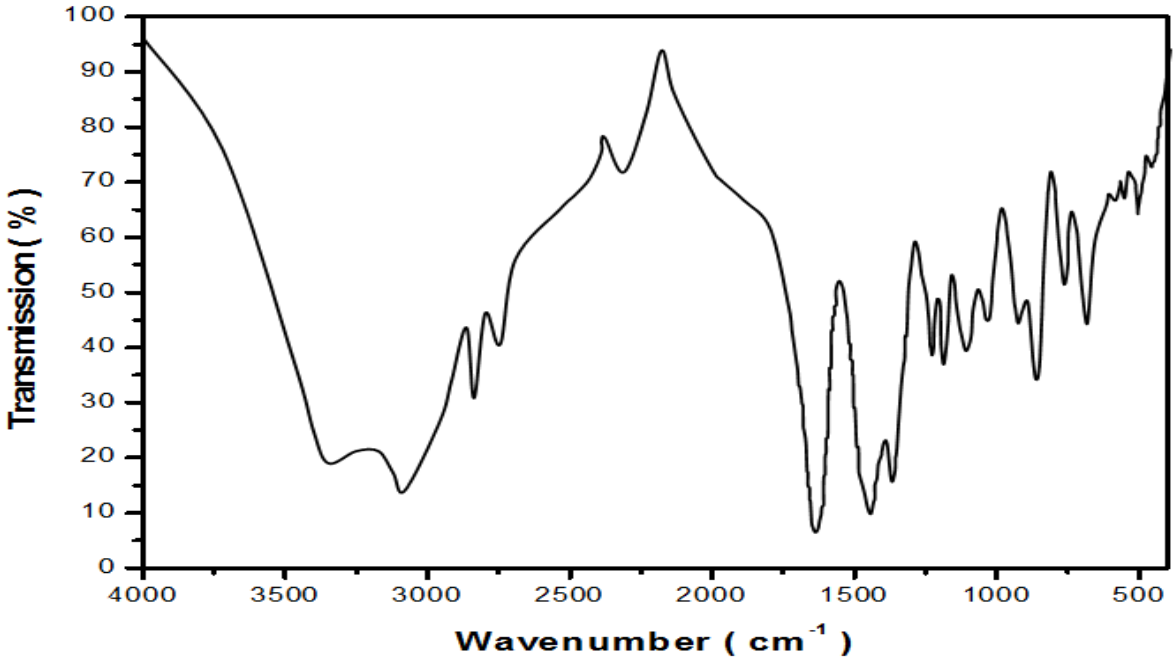

Fig. 3. FT-IR spectrum of LLS

Table 1. FT-IR frequency assignment for LLS

Wave number (cm^{-1})	Assignment
3385	NH_3^+ asymmetric stretching
3091	NH_3^+ symmetric stretching
2830	NH_3^+ symmetric stretching and C-(OH)
2740	C-H symmetric stretching
2417	Overtones and combinations
1620	NH_3^+ and COO^- asymmetric stretching
1432	NH_3^+ rocking
1356	NH_3^+ torsion.
1220	C-O symmetric stretching
1180	C-(OH) symmetric stretching and C-H in plane deformation
1030	C-N stretching,
764	C-N deformation
690	C-C out-of-plane deformation
595	NH_3^+ torsion.

4.3 Optical Absorption Spectrum

Optical window width is an important characteristic of an NLO material. Hence the study of the transmission of UV–vis range through the NLO material is necessary. The optical absorption spectral analysis of LLS was carried out between 190-1100 nm. The spectrum obtained is attributed to the promotion of electrons in σ-, π- and n-orbital from the ground state to higher state. The peak at 290 nm identifies the presence of C = O group. The peaks in the range between 300 to 350 nm, due to n → π* transitions confirmed the presence of carbonyl compound having double bond separated by two or more single bonds. The peak at 250 nm confirmed the presence of C – C bonded system [10]. From the absorption spectrum (Fig. 4), it is clear that the crystal is transparent up to 1100 nm. The crystal has almost less than 0.1 unit of absorption. From the UV–visible spectrum, it is clear that lower cut-off wavelength 235 nm combined with the very good transparency makes the usefulness of this material for optoelectronic and nonlinear optical applications [11]. Absence of absorbance in the region between 300 and 1100 nm is an advantage as it is a key requirement for materials having NLO properties. The absorption coefficient (α) of LLS single crystal was determined from optical absorption measurements, measured at room temperature. The value of 'α' was estimated using the expression $\alpha = -(1/t) \ln (T)$ where T is the transmittance, t is the thickness of the specimen. These absorption coefficient values were used to determine optical energy gap. Using Tauc's relation, a graph has been plotted to estimate the direct band gap value. Fig. 5 shows the plot of $(\alpha h\nu)^2$ versus hν, where α is the optical absorption coefficient and hν is the energy of the incident photon. The direct energy gap (E_{gd}) is determined by extrapolating the straight line portion of the curve to $(\alpha h\nu)^2 = 0$. From this drawing, E_{gd} is found to be 5.3 eV.

4.4. NLO Studies

The second harmonic generation (SHG) conversion efficiency of LLS was measured by the powder Kurtz and Perry [9]. A Q-switched Nd:YAG laser beam of wavelength 1064 nm, with an input power of 10.8 mJ, and pulse width of 8ns with a repetition rate of 10 Hz was used. The grown single crystal of LLS was powdered with a uniform particle size and then packed in a microcapillary of uniform bore and exposed to laser radiations. The output from the sample was monochromated to collect the intensity of 532 nm component. A sample of potassium dihydrogen phosphate (KDP), also powdered was used for the same experiment as a reference material in the SHG measurement. The non-zero measured powder SHG signal is reliable with the SHG activity, which can be correlated with noncentrosymmetric crystal structure. The relative efficiency of LLS with that of KDP has been measured. It is found that the efficiency of the LLS crystal (108 mV), which is two times greater than that of KDP (53 mV). The powder SHG measurements reported previously by V. Krishnakumar et al. [7] indicate that the LLS salt has SHG efficiency 60% to that of KDP. This difference in measured SHG activity may be due to the grain size and packing environment of the sample during SHG study. The level of SHG response of a given material is inherently dependent upon its structural attributes. On a molecular scale, the extent of charge transfer across the NLO chromophore determines the level of SHG output, greater the charge transfer, larger is the SHG output. The presence of strong intermolecular interactions, such as hydrogen bonds can extend this level of charge transfer into the supramolecular realm, owing to their electrostatic and directed nature, thereby enhancing the SHG response [12-13]. The second harmonic generation conversion efficiency of the grown crystal shows the suitability for frequency conversion applications.

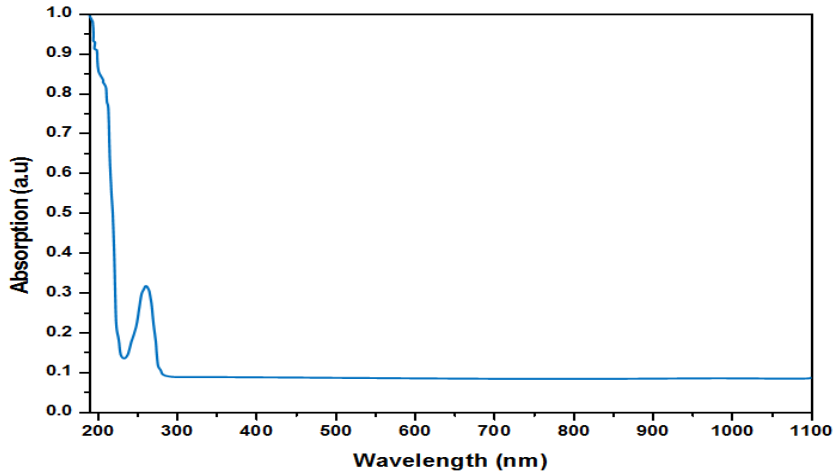

Fig. 4. Optical absorption spectrum of LLS

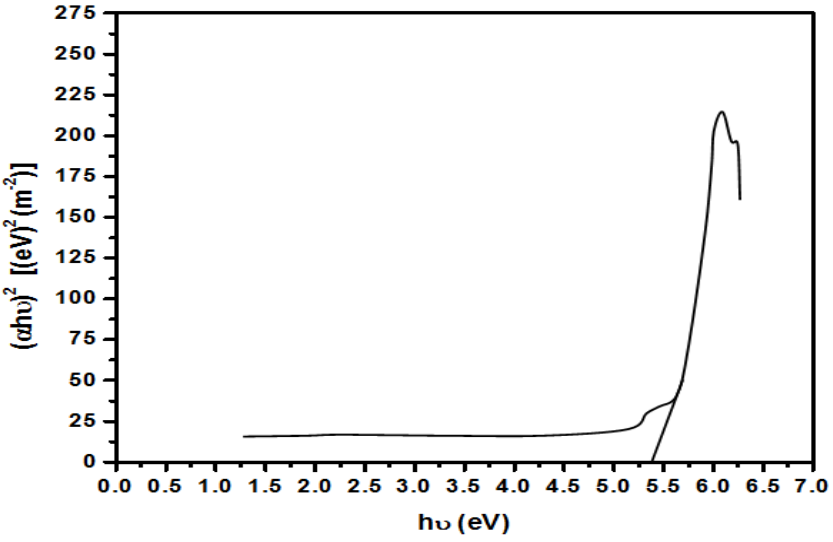

Fig. 5. Tauc's plot of LLS

4.5. Electrical Studies

Dielectric properties are correlated with the electro-optic property of the crystals [14–16]. The magnitude of dielectric constant depends on the degree of polarization charge displacement in the crystals. The dielectric constant

and dielectric loss was measured using HIOKI 3532-50 LCR HITESTER. The selected samples were cut using a diamond saw and polished using paraffin oil. Two opposite surfaces across the breadth of the LLS samples were treated with good quality silver paste in order to obtain good Ohmic contact. The studies were carried out and the capacitance, dielectric loss (tan δ) and *ac* conductivity of the sample as a function of frequency (100 Hz–5 MHz) and temperature (in the range 308, 328, 348 and 368 K). A small cylindrical furnace with dimensions 20 cm x 20 cm x 20 cm, whose temperature was controlled by Eurotherm temperature controller (± 0.01 °C) was used for the experiment. The dielectric constant was calculated using the relation $\varepsilon_r = Cd/\varepsilon_o A$, where ε_o is the permittivity of the free space, C is the capacitance, d is the thickness of the sample and A is the area of cross section. The variation in the dielectric constant with frequency at different temperatures is illustrated in Fig. 6. The dielectric constant has a maximum value in the lower frequency region and then decreases with the applied frequency. The decrease of dielectric constant with increasing frequency is a normal dielectric behavior and this may be due to the presence of all the polarizations, namely space charge, orientation, electronic and ionic polarizations; minimum value at higher frequencies is attributed to the slow loss of significance of these polarizations [17]. The higher values of dielectric loss at low frequencies originate from space charge polarization mechanism dipoles (Fig. 7). The gradual decrease in dielectric constant and dielectric loss with frequency suggests that the grown crystals have varying relaxation times. Dielectric constant and loss increases slowly with temperatures as shown in Figs. 8 and 9. The influence of temperature leads to increase in dielectric constant with increasing temperature and is due to the presence of electronic polarization. The characteristic of low dielectric loss at high frequencies classifies that the grown sample possess enhanced optical quality with lesser defects [18-20]. Usually the dielectric losses fall into two categories, they are intrinsic and extrinsic. Intrinsic losses are dependent on the crystal structure and can be described by the interaction of the phonon system with the ac electric field. The ac electric field alters the equilibrium of the phonon system and the subsequent relaxation is associated with energy dissipation. These intrinsic losses set the lower limit of losses found in pure ‘‘defect-free’’ single crystals. Extrinsic losses are associated with imperfections in the crystal, e.g., impurities, microstructural defects, grain boundaries, porosity, microcracks and random crystallite orientation. Low value of dielectric loss suggests that the LLS crystal possesses enhanced optical quality with low density of defects.

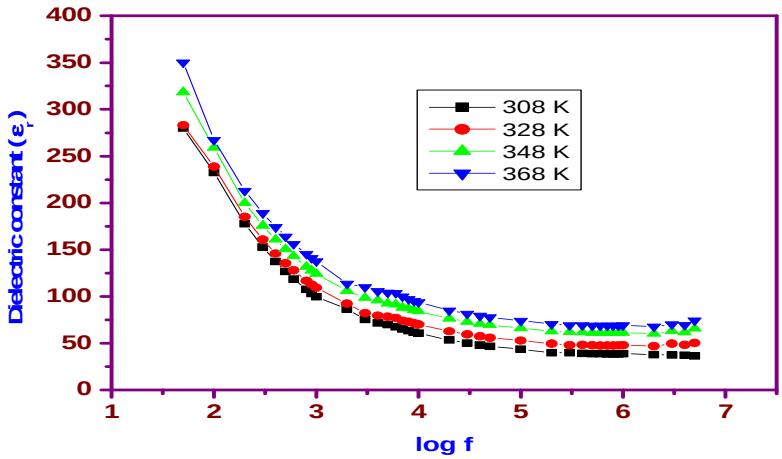

Fig. 6. Variation of dielectric constant with log frequency at different temperatures for LLS single crystal

The variation of *ac* conductivity with frequency at different temperatures is shown in Fig. 10. It is clear that the conductivity increases with increasing frequency and can be expressed as $\sigma_{ac} = \omega\varepsilon_r \tan\delta\varepsilon_o$ and, where $\omega=2\pi f$. It is observed that at a given temperature, the magnitude of conductivity is high at higher frequencies, there by supporting the small polaron hopping model [21]. The electrical conduction is mainly a defect controlled process in low temperature region. It is observed from Fig. 10 that the electrical conduction of LLS is low at low temperature owing to trapping of some carriers at defect sites. As temperature rises, more and more defects are created, and as a result, the conductivity increases, which is predominantly due to moment of defects produced by thermal activation. The Arrhenius plot of *ln* σ_{ac} versus 1000/T is shown in Fig. 11. The line of best fit for the plot of *ln* σ_{ac} versus 1000/T obeys Arrhenius relationship $\sigma_{ac} = \sigma_o \exp(-E_a/kT)$ where σ_o is the pre-exponent factor, E_a the activation energy for the conduction process and k is the Boltzman constant. Therefore, the sample exhibits Arrhenius type conductivity behaviour in the temperature range of investigation. From the graph, the value of *ac* activation energy for ionic migration was estimated (Fig. 12).

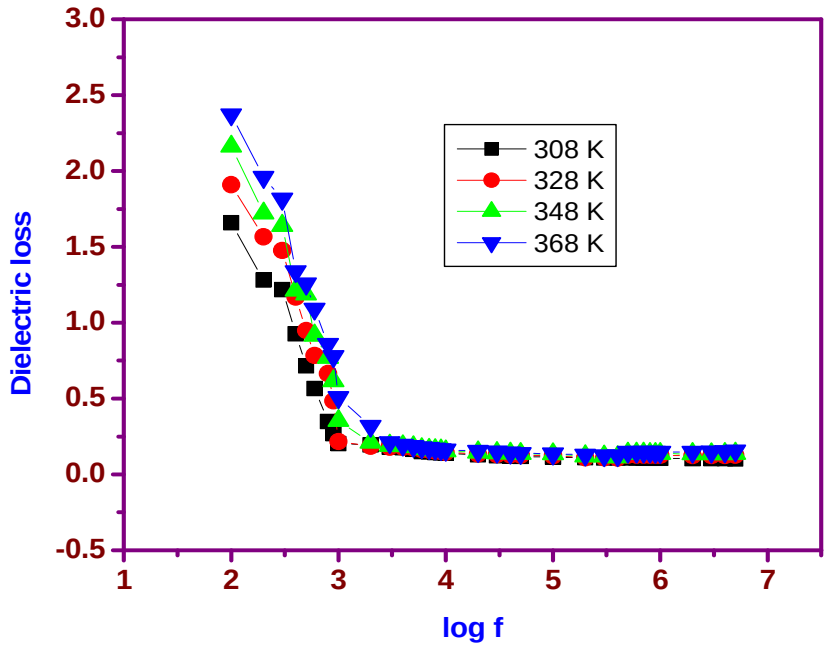

Fig. 7. Variation of dielectric loss with log frequency at different temperatures for LLS single crystal

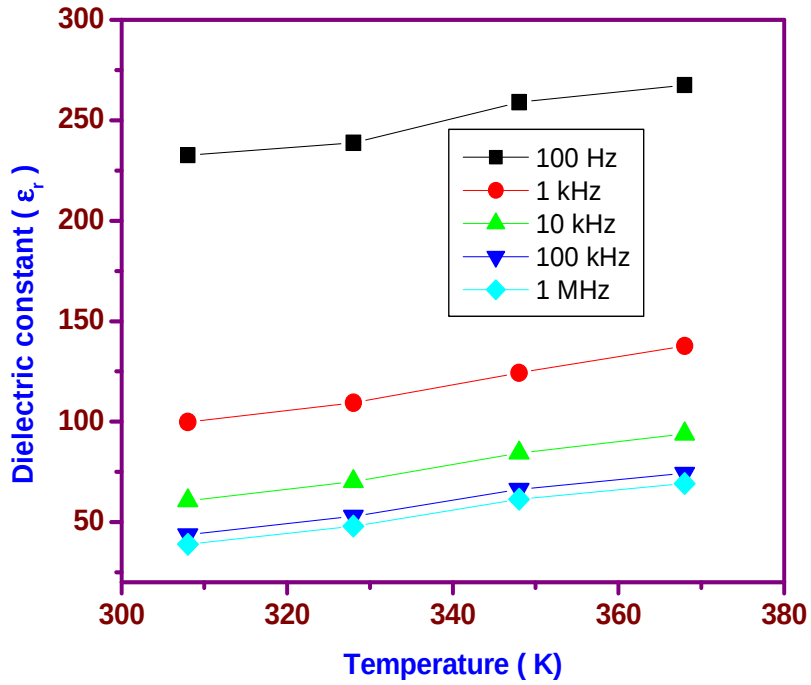

Fig. 8. Temperature dependence of dielectric constant for LLS single crystal

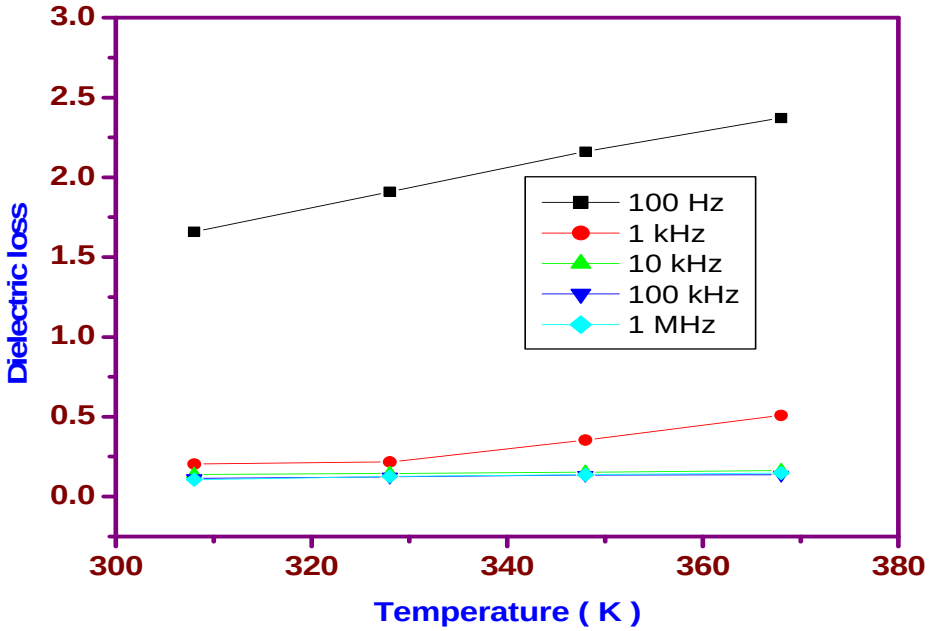

Fig. 9. Temperature dependence of dielectric loss for LLS single crystal

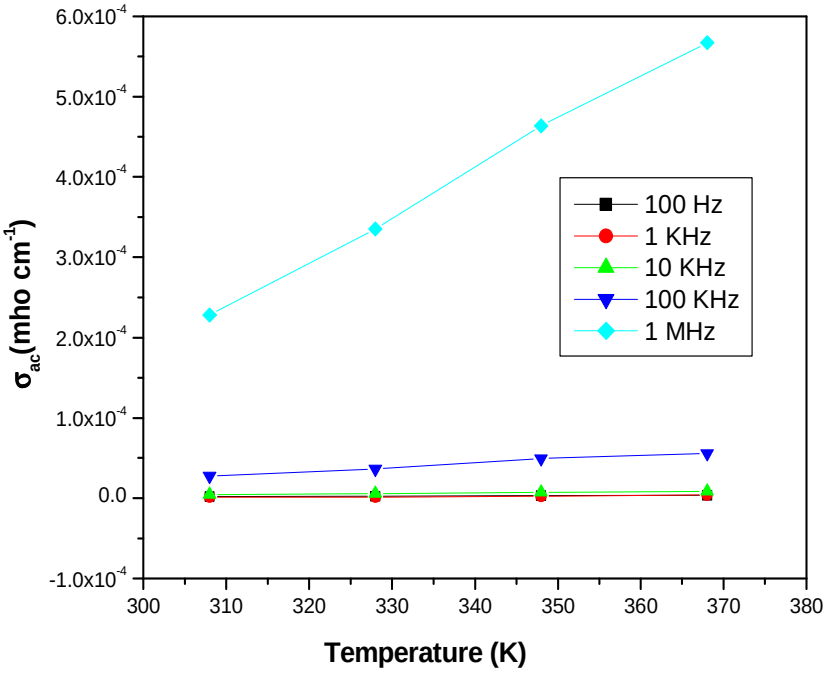

Fig. 10. The *ac* electrical conductivities for LLS crystal

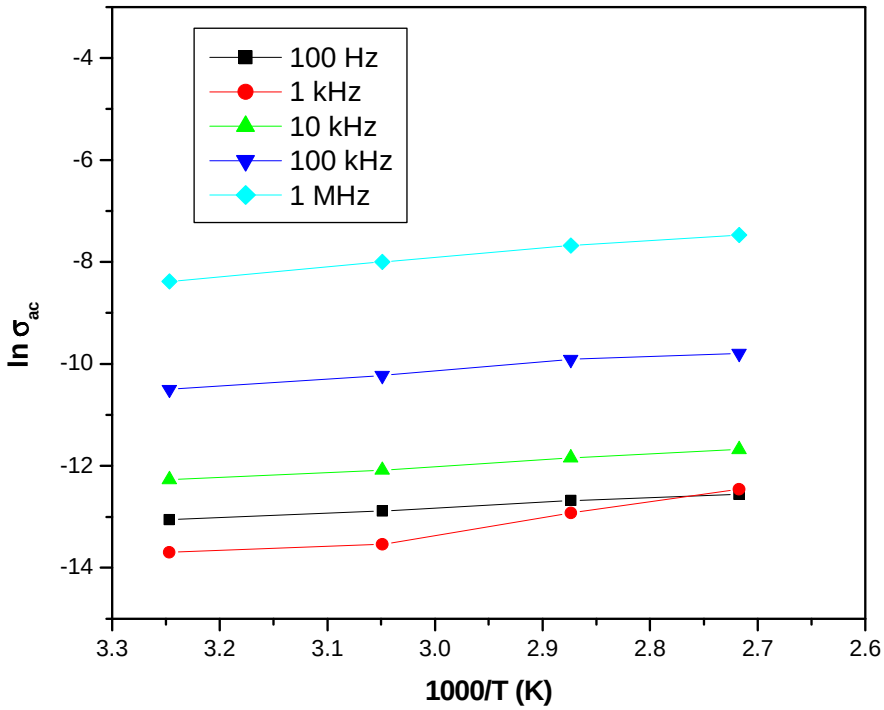

Fig. 11. Plot of ln(σ_{ac}) versus 1000/T for LLS single crystal

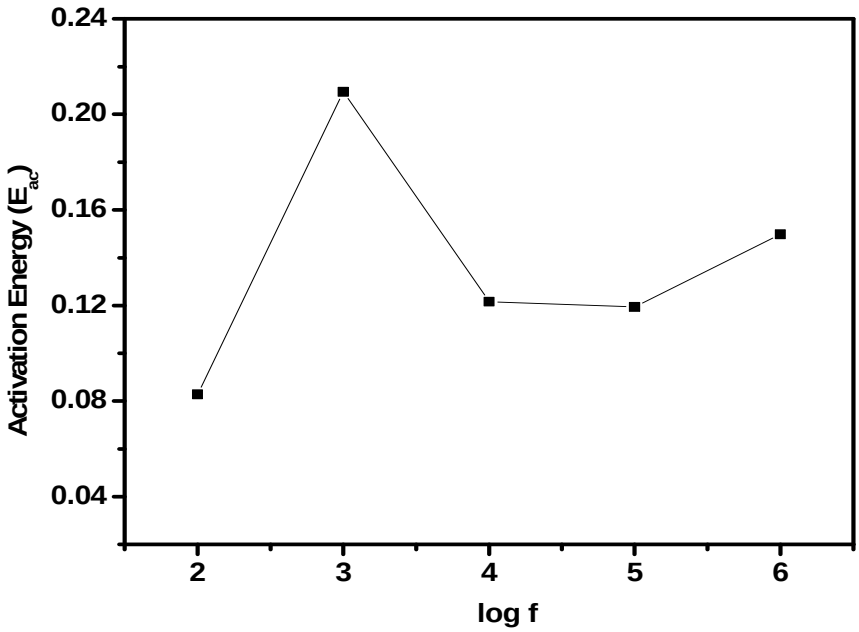

Fig. 12. Frequency dependence of *ac* activation energy for LLS single crystal

The conductivity measurements were carried out for the LLS crystal using the conventional two-probe technique at different temperatures ranging from 308 to 368 K. The *dc* electrical conductivity (σ_{dc}) of the crystal was calculated using the relation

σ_{dc}= t/RA

where R is the measured resistance, t is the thickness of the sample and A is the area of face in contact with the electrode. Well sized crystal of LLS was used for conductivity study. The σ_{dc} values were fitted into the equation $\sigma_{dc} = \sigma_o \exp(-E_d/kT)$

Fig. 13 represents the temperature dependence of conductivity of the sample is found to increase with increase in temperature. The value of conductivity σ_{dc} is found to increase with temperature. The conduction region considered in the present study seems to be connected to mobility of vacancies. The *dc* activation energy of the LLS crystal is found to be 0.081 eV (Fig. 14). The low activation energies observed suggests that oxygen vacancies may be responsible for conduction in the region.

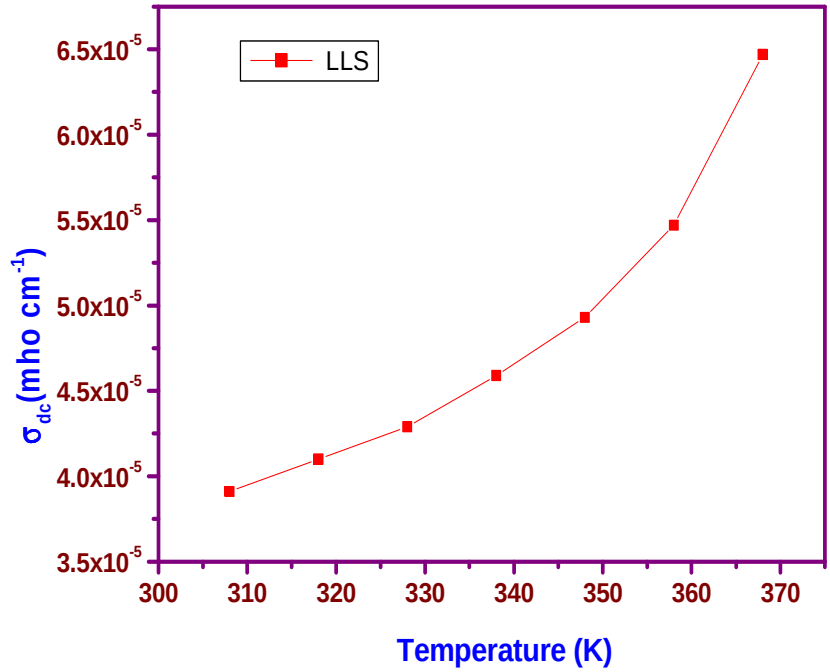

Fig. 13. The *dc* electrical conductivities for LLS crystal

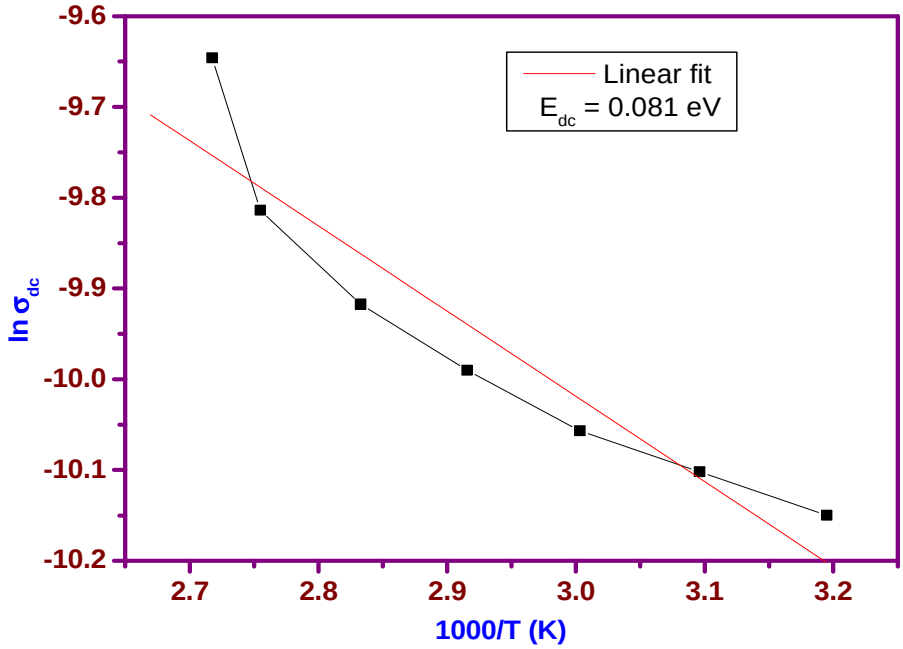

Fig. 14. Plot of ln(σ_{dc}) versus 1000/T for LLS single crystal

4.6. Photoconductivity Study

The photoconductivity study was carried out using Keithley 480 picoammeter. Polished sample of LLS was attached to microscope slide, and two electrodes of thin copper wire (0.15 cm diameter) were fixed by use of silver paint. The details of the experimental set-up used in the present study are reported elsewhere [22]. Initially, the sample is kept away from any other radiations. Dark current is measured by connecting the sample in series to a DC power supply and picoammeter. Electrical contacts are made on the sample using silver paint. The photocurrent for the same sample is measured by exposing it to the radiation from a halogen lamp containing iodine vapour by focusing a spot of light on the sample with the help of a convex lens. The variation of both dark and photocurrents with applied field is shown in Fig. 15. It is seen from the plot that both the dark and photocurrents of the sample increase linearly with the applied field. The photocurrent is seen to be less than the dark current for the same applied field, which reveals the negative photoconducting behaviour of the sample. However, in the present work, the negative photoconductivity exhibited by the LLS sample may be due to the reduction in the number of charge carriers in the presence of radiation [23-24]. The stockman model explains the tendency of decrease in mobile charge carriers during negative photoconductivity [25]. According to this model, negative photoconductivity is based on a two-level scheme. One level is located between the Fermi level and the conduction band while the other is situated close to the valence band. The second state has high capture cross-sections for electrons and holes. This state can capture electrons from the conduction band and holes from the valance band, which the net number of mobile charge carriers decreased due to the presence of radiation, giving negative photoconductivity.

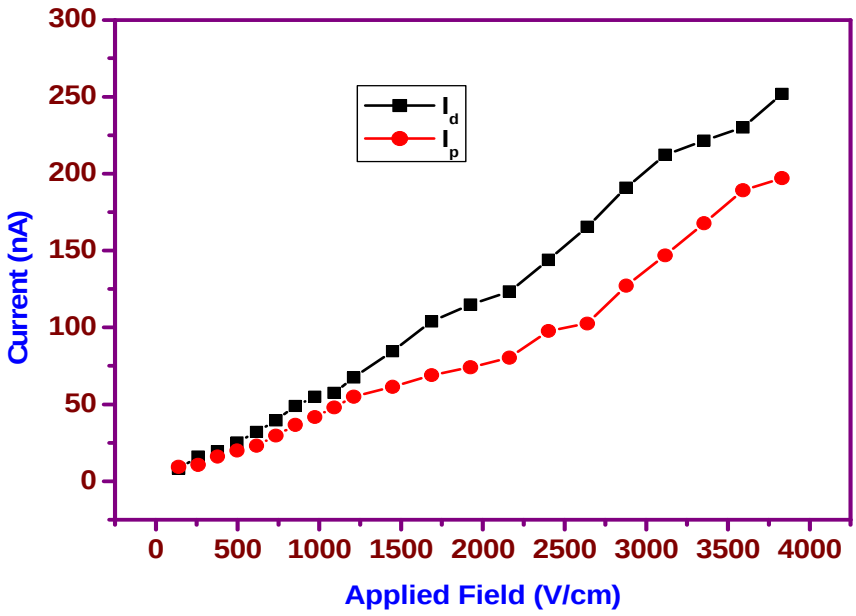

Fig. 15. Field dependent photoconductivity of LLS single crystal

CONCLUSION

In the present study, optically good quality single crystals of LLS are conveniently grown in acetone-water mixed solvent system by slow solvent evaporation method. The single crystal XRD data proves that LASP crystal belongs to orthorhombic in structure with a noncentrosymmetric space group $P2_12_12_1$. Various functional groups present in the grown crystal were identified by FT-IR studies. Optical absorption studies confirm the UV cut-off wavelength of LLS at 235 nm. The band gap energy of the sample is calculated and it is found to be 5.3 eV. The studies on NLO property confirmed the second harmonic conversion efficiency of the crystal to be comparable to better than KDP. The variation of dielectric constant and dielectric loss are studied with varying frequency at different temperature. The photoconductivity study reveals that the LLS crystal exhibits negative photoconductivity. The activation energy of the sample is calculated by *ac/dc* conductivity studies. Thus, the optical, NLO and electrical properties of the crystal indicate the suitability of this crystal for photonic device fabrication.

REFERENCES

[1]Hann RA, Bloor D., *Organic materials for nonlinear optics*. The Royal Society of Chemistry Special Publications, **1989**.

[2]Dmitriev VG, Gurzadyan GG, Nicogosyan DN., Handbook *of nonlinear optical crystals*, New York: Springer-verlag, **1999**.
[3]Prasad Paras N, Williams David J., *Introduction to nonlinear optical effect in molecules and polymers*. John Wiley & Sons Inc, **1991**.
[4]Bhat MN, Dharmaprakash SM., *J. Cryst. Growth*, **2002**, 236, 379.
[5]Eimerl D., Velsko S., Davis L., Wang F., G. Loicono G., Kennedy G., *IEEE*, J. Quantum Electron., **1989**, 25, 179.
[6]Marchewka M K, Debrus S and Ratajczak H, *Cryst. Growth Des*., **2003**, 3, 587
[7]Krishnakumar V., Manohar S., Nagalakshmi R., *Spectrochimica Acta Part A*, **2010**, 75, 1394.
[8]Capasso S., Mattia C.A., Mazzarella L., Zagari A., *Acta Cryst. C*, **1983**, 39, 281.
[9] Kurtz S.K., Perry T.T., *J. Appl. Phys*., **1968**, 39, 3798.
[10] Furniss A., Hannaford B., Smith C., Tatchell D., *Vogel's Text book of practical organic chemistry*, ELBS 5th edition, **1989**.
[11] Martin Britto Dhas S.A., Natarajan S., *Cryst. Res. Technol.*, **2008**, 43, 869.
[12] Oudar J.L., *J. Chem. Phys*., **1977**, 67, 446.
[13] Oudar J.L., J. Zyss, *Phys. Rev. A*, **1982**, 26, 2028.
[14] Boomadevi S., Dhanasekaran R., *J. Cryst. Growth*, **2004**, 261, 70.
[15] Dongfeng Xue, Siyuan Zhang, *Physica B*, **1999**, 262, 78.
[16] Dongfeng Xue, Kenji Kitamura, *Jpn. J. Appl. Phys*., **2003**, 42, 6230.
[17]Reicha F.M., El-Hiti M., El-Sonabati A.Z., Diab M.A., *J. Phys. D: Appl. Phys*., **1991**, 24, 369.
[18] Smyth C.P., *Dielectric Behaviour and Structure*, Mc Graw Hill, New York, **1995**.
[19] Balarew C., Duhlew R., *J. Solid State Chem*., **1984,** 55, 1.
[20] Yogam F., Vetha Potheher I., Cyrac Peter A., Tamilselvan S., Leo Rajesh A. Vimalan M., Sagayaraj P., *Advances in Applied Science Research*, **2011**, 2 (1) 261.
[21] Varma K.B.R., Ramanaiah K.V., Rao K.V., *Bull. Mater. Sci.***, 1983,** 5, 39.
[22] Francis P. Xavier, Anto Regis Inigo and George J. Goldsmith, *J. Porphyrins Phthalocyanines*, **1999,** 3, 679.
[23] Bube R.H., *Photoconductivity of Solids*, Wiley Interscience, New York, **1960**.
[24] Abraham Rajasekar S., Thamizharasan K., Joe G.M. Jesudurai., Prem Anand D., Sagayaraj P., *Mater. Chem. Phys*., **2004,** 84, 157.
[25] Joshi V.N., *Photoconductivity*, Marcel Dekker, New York, **1990**.